

Fast migration of low-mass planets in radiative discs

A. Pierens^{1,2}

¹*Université de Bordeaux, Observatoire Aquitain des Sciences de l'Univers, BP89 33271 Floirac Cedex, France*

²*CNRS, Laboratoire d'Astrophysique de Bordeaux, BP89 33271 Floirac Cedex, France*

Released 2012 Xxxxx XX

ABSTRACT

Low-mass planets are known to undergo Type I migration and this process must have played a key role during the evolution of planetary systems. Analytical formulae for the disc torque have been derived assuming that the planet evolves on a fixed circular orbit. However, recent work has shown that in isothermal discs, a migrating protoplanet may also experience dynamical corotation torques that scale with the planet drift rate. The aim of this study is to examine whether dynamical corotation torques can also affect the migration of low-mass planets in non-isothermal discs. We performed 2D radiative hydrodynamical simulations to examine the orbital evolution outcome of migrating protoplanets as a function of disc mass. We find that a protoplanet can enter a fast migration regime when it migrates in the direction set by the entropy-related horseshoe drag and when the Toomre stability parameter is less than a threshold value below which the horseshoe region contracts into a tadpole-like region. In that case, an underdense trapped region appears near the planet, with an entropy excess compared to the ambient disc. If the viscosity and thermal diffusivity are small enough so that the entropy excess is conserved during migration, the planet then experiences strong corotation torques arising from the material flowing across the planet orbit. During fast migration, we observe that a protoplanet can pass through the zero-torque line predicted by static torques. We also find that fast migration may help in disrupting the mean-motion resonances that are formed by convergent migration of embryos.

Key words: accretion, accretion discs – planet-disc interactions – planets and satellites: formation – hydrodynamics – methods: numerical

1 INTRODUCTION

A striking feature of the population of exoplanets discovered so far is their great diversity. Compact and non-resonant systems of super-Earths and mini-Neptunes have been discovered orbiting within a few tenths of AU from their stars (e.g. Lissauer et al. 2011; Lovis et al. 2011). Giant planets with periods from days to several thousands of days have also been found around $\sim 14\%$ of Sun-like stars, with a frequency that is strongly correlated to the metallicity of the host star (Cumming et al. 2008; Mayor et al. 2011). A main aim of planet formation and evolution scenarios is to examine whether this broad diversity can be explained, and under which conditions. These scenarios can be constrained using for example planet population syntheses which combine analytical models of disc evolution, planet formation and orbital evolution due to disc-planet interactions (Ida & Lin 2008; Mordasini et al. 2009; Mordasini et al. 2012); and generate a large variety of system architectures that can be statistically compared to observations. An alternative method is to make use of N-body simulations of planetary systems formation which do not cover a parameter space as large as in planet population syntheses, but allow for a self-consistent treatment of planet-planet interac-

tions (Hellary & Nelson 2012; Coleman & Nelson 2014; Cossou et al. 2014).

In both of these approaches, disc-planet interactions causing planet migration are modeled using analytical formulae for the disc torque experienced by the planet. This gravitational torque consists of two components. The differential Lindblad torque results from the angular momentum exchange between the planet and the spiral density waves it generates inside the disc. For sufficiently low-mass planets, it scales linearly with disc mass and planet mass and as the inverse square of the disc aspect ratio (Tanaka et al. 2002). Although its sign depends on the density and temperature gradients inside the disc, the differential Lindblad torque is generally negative for typical disc models and is therefore responsible for inward migration. The corotation torque is due to the torque exerted by the material located in the coorbital region of the planet. It is composed of a barotropic part which scales with the vortensity (i.e. the ratio between the vertical component of the vorticity and the disc surface density) gradient (Goldreich & Tremaine 1979) plus an entropy-related part which scales with the entropy gradient (Baruteau & Masset 2008; Paardekooper & Papaloizou 2008). A negative vortensity (resp. entropy) gradient gives rise to a positive vortensity (resp. entropy) related corotation torque. It

has been shown that for mildly positive surface density gradients or negative entropy gradients, a positive corotation torque can eventually counteract the effect of a negative differential Lindblad torque, which may stall or even reverse migration (Masset et al. 2006; Paardekooper & Papaloizou 2009). In isothermal discs, the corotation torque is a non-linear process generally referred as the horseshoe drag and whose amplitude is controlled by advection and diffusion of vortensity inside the horseshoe region. In non-isothermal discs, the corotation torque is also powered by singular production of vortensity due to an entropy discontinuity on downstream separatrices (Masset & Casoli 2009; Paardekooper et al. 2010). In the absence of any diffusion processes inside the disc, vortensity and entropy gradients across the horseshoe region tend to flatten through phase mixing, which causes the two components of the horseshoe drag to saturate. Consequently, desaturating the horseshoe drag requires that some amount of viscous and thermal diffusions are operating inside the horseshoe region. In that case, the amplitude of the horseshoe drag depends on the ratio between the diffusion timescales and the horseshoe libration timescale and its optimal value, also referred as the fully unsaturated horseshoe drag, is obtained when the diffusion timescales are approximately equal to half the horseshoe libration time (e.g. Baruteau & Masset 2013). In the limit where the diffusion timescales become shorter than the U-turn timescale, the corotation torque decreases and approaches the value predicted by linear theory. Therefore, the corotation torque can be considered as a linear combination of the fully unsaturated horseshoe drag and the linear corotation torque with coefficients depending on the ratio between the diffusion timescales and the horseshoe libration timescale. Corotation torque formulae as a function of viscosity and thermal diffusivity were recently proposed by Paardekooper et al. (2011) and Masset & Casoli (2010).

Such analytical formulae have been derived assuming that the planet evolves on a fixed circular orbit. In that case, the planet feels a static torque that depends only on the local temperature and surface density conditions in the disc. If the planet is allowed to migrate, however, the disc torque can also exhibit, under certain conditions, a dependence on the planet drift rate. For instance, this can occur if the planet is massive enough to partly deplete its coorbital region. In that case, a coorbital mass deficit is created and the corotation torque is essentially due to the gas material that flows across the planet's horseshoe region as the latter migrates. This contribution to the corotation torque not only scales with the planet drift rate, but also has the same sign as the drift rate. This yields a positive feedback on migration, and eventually gives rise to runaway effects if the disc is massive enough (Masset & Papaloizou 2003).

In a recent study, Paardekooper (2014) has shown that low-mass planets embedded in isothermal discs a few times more massive than the Minimum Mass Solar Nebula (hereafter MMSN; Hayashi 1981) may also experience runaway migration in some cases. For low-mass planets that do not significantly perturb the underlying disc structure, this process does not result from a coorbital mass deficit but rather arises due to the action of dynamical corotation torques that scale with the planet drift rate and depend on the vortensity gradient inside the disc (Paardekooper 2014). In the case where the migration proceeds in the direction set by the corotation torque, Paardekooper (2014) has shown that these dynamical torques have a positive feedback on migration, and can possibly give rise to high drift rates. Interestingly, using an isothermal disc model with a positive surface density gradient to mimic what may happen in non-isothermal disc, Paardekooper (2014) has shown that an outward migrating protoplanet subject to strong dynamical torques can pass through the location of the zero-torque

radius where the Lindblad torque and the (static) corotation torque cancel each other.

In this paper, we focus on the case of non-isothermal disc models, in which outward migration can proceed due to the operation of the entropy-related horseshoe drag. The aim of this study is to examine the plausibility that low-mass planets embedded in non-isothermal discs experience strong dynamical corotation torques as they migrate. Using hydrodynamical simulations, we find that in relatively massive discs with an initial large-scale entropy gradient, the drift rates reached by a migrating planet can indeed be significantly higher than those expected by assuming a static torque. We show that this occurs when i) the planet migrates in the direction set by the entropy-related horseshoe drag, and ii) the Toomre stability parameter is less than a critical value that depends on the entropy gradient. Below this value, the horseshoe region does not extend to the full 2π in azimuth and an underdense trapped region appears which causes the planet to undergo large drift rates. In this fast migration regime, we also find that an outward migrating protoplanet can migrate well beyond the location of the zero-torque radius, similarly to the findings of Paardekooper (2014) in isothermal discs.

This paper is organized as follows. In Sect. 1, we present the numerical setup. In Sect. 2, we present the results of the simulations for non-isothermal disc models. The case of radiative disc models that include the effects of viscous plus stellar heating, and radiative cooling are discussed in Sect. 3. Finally, we discuss our results and draw our conclusions in Sect. 4.

2 THE HYDRODYNAMICAL MODEL

Simulations were performed using the GENESIS (De Val-Borro et al. 2006) numerical code which solves the equations governing the disc evolution on a polar grid (R, ϕ) using an advection scheme based on the monotonic transport algorithm (Van Leer 1977). It uses the FARGO algorithm (Masset 2000) to avoid time step limitation due to the Keplerian velocity at the inner edge of the disc.

We adopt computational units such that the mass of the central star is $M_* = 1M_\odot$, the gravitational constant is $G = 1$, and the radius $R = 1$ in the computational domain corresponds to 5.2 AU. When discussing the results of the simulations, time will be measured in units of the orbital period at $R = 1$.

We do not consider the disc self-gravity in this work. The typical value for the Toomre stability parameter $Q = \kappa c_s / \pi G \Sigma$, where κ is the epicyclic frequency, c_s the sound speed and Σ the surface density is $Q \sim 3 - 4$, suggesting thereby that the effect of self-gravity may be important. The gravitational potential for the disc therefore restricts to the gravitational potential from the star and the planet, plus the indirect terms that account for the fact that the frame centered on the star is not inertial. The gravitational potential of the planet is smoothed over a distance $b = 0.4H_p$, where H_p is the disc scale height at the location of the planet. Here, the planet orbit can evolve due to the gravitational forces exerted by the star and the disc, and eventually due to the gravitational interaction of the planet with other bodies (see Sect. 4.2). When calculating the disc force experienced by the planet, we follow Paardekooper (2014) and exclude the axisymmetric component of the force to ensure consistency as the planet migrates.

In the following, two different forms of the energy equation will be employed. We will first consider non-isothermal disc models for which the energy equation corresponds to an advection-diffusion equation for the gas entropy with a constant thermal diffusion coefficient (Paardekooper et al. 2011). Then we will focus

on more realistic, radiative disc models whose thermal structure results from the balance between viscous plus stellar heating, and radiative cooling.

2.1 Non-isothermal discs

2.1.1 Numerical setup

For non-isothermal disc models, we solve the following energy equation:

$$\frac{\partial e}{\partial t} + \nabla \cdot (e\mathbf{v}) = -(\gamma - 1)e\nabla \cdot \mathbf{v} + \chi e \nabla^2 \log S \quad (1)$$

where e is the thermal energy density, \mathbf{v} the velocity, γ the adiabatic index which is set to $\gamma = 1.4$, and where χ is a thermal diffusion coefficient. In the previous equation, $S = p/\Sigma^\gamma$ is the gas entropy, with $p = (\gamma - 1)e$ the gas pressure. Strictly speaking, the diffusion term in the previous equation should involve the laplacian of temperature rather than entropy. This form for the energy equation is used so that it corresponds to an advection-diffusion equation for the gas entropy, and is valid provided that the variations in temperature occur over a scale smaller than those corresponding to the gas pressure (Masset & Casoli 2010). Here, this condition is fulfilled since we are interested in low-mass planets for which the width of the horseshoe region is typically a fraction of the disc pressure scale height. The thermal diffusion coefficient χ is chosen assuming a Prandtl number $P_R = \nu/\chi$ of unity, where ν is the kinematic viscosity which is assumed to be constant. In the case where diffusion of entropy is due to turbulent transport, this is consistent with the results of Pierens et al. (2012) who found $P_R \sim 1.2$ in non-isothermal disc models with turbulence driven by stochastic forcing. In a real protoplanetary disc, however, where radiative diffusion can possibly dominate over turbulent transport for diffusing entropy, we expect the Prandtl number to be of the order of unity only in the optically thick inner regions (Pierens et al. 2012), while a value $P_r < 1$ is expected in the outer, optically thin regions.

Typically $N_R = 1600$ radial grid cells uniformly distributed between $R_{in} = 0.4$ and $R_{out} = 5$ are used, and $N_\phi = 2130$ azimuthal grid cells.

We employ closed boundary conditions at both the inner and outer edges of the computational domain, and make use of wave-killing zones for $R < 0.5$ and $R > 4.5$ to avoid wave reflections at the disc edges.

2.1.2 Initial conditions for the non-isothermal runs

The initial disc surface density is $\Sigma = \Sigma_0(R/a_0)^{-\sigma}$, where Σ_0 is the surface density at the initial position of the planet $R = a_0$ and where the power law index is such that $\sigma = 3/2$ by default. For such a disc surface density profile, the initial vortensity-related part of the corotation torque cancels out so that the corotation torque consists only of its entropy-related part. Following Paardekooper (2014), we parametrise the disc mass through the parameter

$$q_d = \frac{\pi a_0^2 \Sigma_0}{M_\star},$$

for which we adopt values ranging from $q_d = 0.005$ to $q_d = 0.03$.

The initial aspect ratio is $h = h_0(R/a_0)^f$ where $h_0 = 0.05$ and f is the disc flaring index for which we consider values of $f = 0.7$ and $f = -0.8$. This corresponds to initial temperature profiles that vary as $R^{-\beta}$ with $\beta = 1 - 2f = -0.4$ and $\beta = 2.6$ respectively, and to initial entropy profiles that vary as $R^{-\xi}$ with $\xi = \beta - (\gamma - 1)\sigma = -1$ and $\xi = 2$ respectively.

Our reference value for the planet-to-star mass ratio is $q = 10^{-5}$ (equivalent to a 3.3 Earth mass planet in our units). For $h_0 = 0.05$, the half-width of the horseshoe region is $x_s \sim 1.1a_0 \sqrt{q/h_0} \sim 0.016 a_0$ (Masset et al. 2006), which means that the horseshoe region is typically resolved by about 12 grid cells in the radial direction.

2.2 The radiative disc model

2.2.1 Numerical setup

In addition to these non-isothermal disc models, we have also considered more realistic discs in which the effects of viscous and stellar heating are balanced by radiative cooling. In that case, the following energy equation is adopted:

$$\frac{\partial e}{\partial t} + \nabla \cdot (e\mathbf{v}) = -(\gamma - 1)e\nabla \cdot \mathbf{v} + Q_{vis}^+ - Q^- - 2H\nabla \cdot \mathbf{F} \quad (2)$$

where H is the disc scale height. In the previous equation, Q_{vis}^+ is the viscous heating term, $Q^- = 2\sigma_B T_{eff}^4$ is the local radiative cooling from the disc surfaces, where σ_B is the Stephan-Boltzmann constant and T_{eff} the effective temperature which is given by (Menou & Goodman 2004):

$$T_{eff}^4 = \frac{T^4 - T_{irr}^4}{\tau_{eff}} \quad \text{with} \quad \tau_{eff} = \frac{3}{8}\tau + \frac{\sqrt{3}}{4} + \frac{1}{4\tau} \quad (3)$$

Here, T is the midplane temperature and $\tau = \kappa\Sigma/2$ is the vertical optical depth, where κ is the Rosseland mean opacity which is taken from Bell & Lin (1994). T_{irr} is the irradiation temperature which is computed from the irradiation flux (Menou & Goodman 2004):

$$\sigma_B T_{irr}^4 = A \frac{L_\star(1 - \epsilon) H}{4\pi R^2} \frac{1}{R} \left(\frac{d \log H}{d \log R} - 1 \right) \quad (4)$$

where $\epsilon = 1/2$ is the disc albedo and L_\star the stellar luminosity which is computed assuming a stellar radius $R_\star = 1.5 R_\odot$ and a stellar temperature $T_\star = 4370$ K. The factor A is set to $A = 1$ if $d(H/R)/dR > 0$, whereas we set $A = 0$ in the regions where $d(H/R)/dR < 0$ in order to take into account possible self-shadowing effects (Gunther & Kley 2004). In Eq. 2, \mathbf{F} is the radiative flux which is treated in the flux-limited diffusion approach and which reads (e.g. Kley & Crida 2008):

$$\mathbf{F} = -\frac{16\sigma\lambda T^3}{\rho\kappa} \nabla T \quad (5)$$

where $\rho = \Sigma/2H$ is the mid plane density and where λ is a flux-limiter (e.g. Kley 1989).

2.2.2 Initial conditions for the radiative runs

For the radiative simulations, we will focus on the case of equilibrium discs with surface density $\Sigma = \Sigma_0(R/R_0)^{-1/2}$ and constant viscosity, where Σ_0 is the surface density at $R_0 = 1$. Two disc models are considered, with parameters summarized in Table 1. For Model 1, $\Sigma_0 = 1.6 \times 10^{-3}$ (equivalent to $\Sigma_0 = 520 \text{ g.cm}^{-2}$ at 5.2 AU) and $\nu = 10^{-5}$, whereas for Model 2, $\Sigma_0 = 3.2 \times 10^{-3}$ (equivalent to $\Sigma_0 = 1024 \text{ g.cm}^{-2}$ at 5.2 AU) and $\nu = 10^{-6}$.

The resolution used in each simulation is $(N_R, N_\phi) = (1024, 1536)$ with a radial extent corresponding to $R \in [R_{in}, R_{out}]$, where R_{in} and R_{out} are given in Table 1.

We adopt planet masses such that $q = 3 \times 10^{-5}, 6 \times 10^{-5}, 10^{-4}$ for Model 1 and $q = 10^{-5}, 1.5 \times 10^{-5}, 2 \times 10^{-5}$ for Model 2. For each model, the planet's horseshoe region is resolved at minimum by

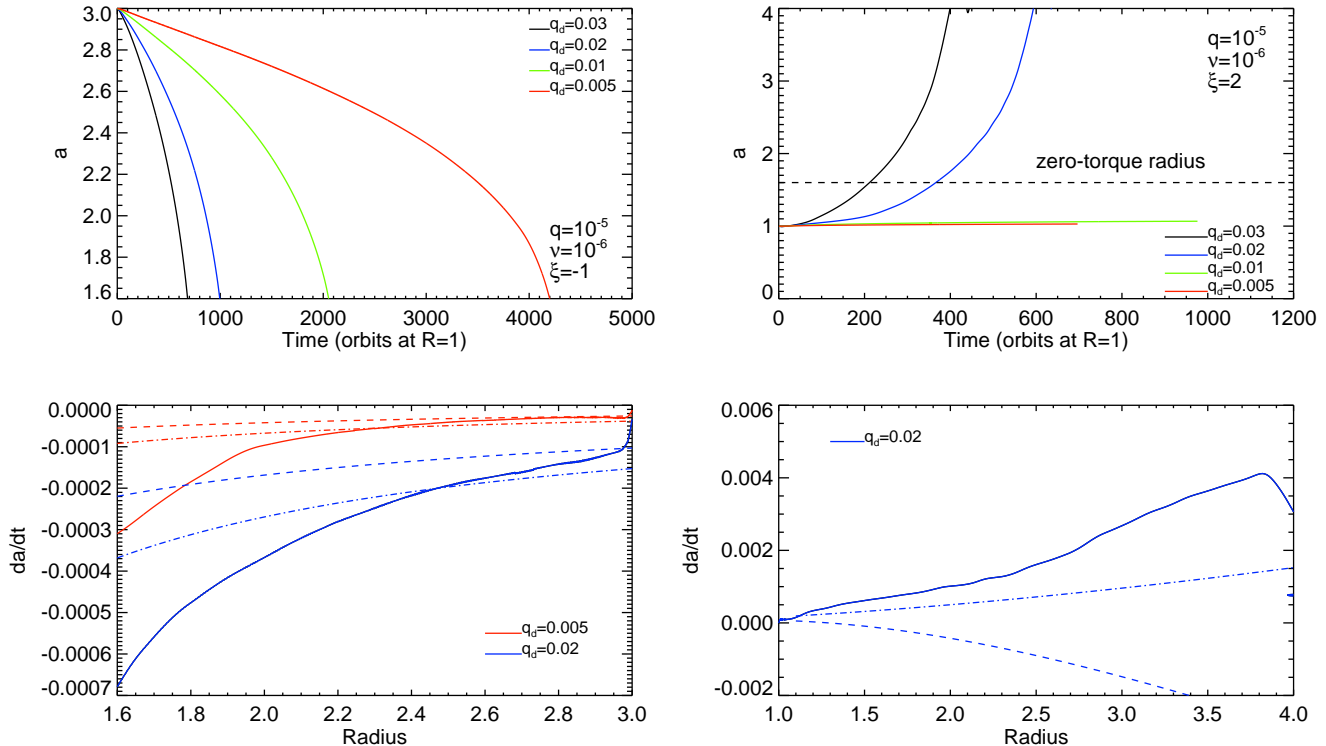


Figure 1. *Left panel:* Time evolution of the semi-major axis (top) and drift rate as a function of radius (bottom) of a protoplanet with $q = 10^{-5}$ embedded in a non-isothermal disc with $\xi = -1$ and $\nu = \chi = 10^{-6}$, for various disc masses. The dashed line shows the drift rate that is expected from analytical formulae for the disc torque, whereas the dot-dashed line corresponds to the drift rate expected assuming a fully unsaturated entropy-related horseshoe drag. *Right panel:* same but for an initial entropy gradient corresponding to $\xi = 2$.

Table 1. Parameters of the radiative simulations, where $\Sigma = \Sigma_0(R/R_0)^{-1/2}$ and where the viscosity is constant

Model	Σ_0	ν	R_{in}	R_{out}
Model 1	1.6×10^{-3}	10^{-5}	0.4	6
Model 2	3.2×10^{-3}	10^{-6}	0.4	3.5

~ 11 grid cells along the radial direction, which leads to a relative error on the estimation of the corotation torque of $\sim 10\%$ (Masset 2002).

3 NON-ISOTHERMAL DISC MODELS

3.1 Results

For a surface density profile with $\sigma = 1.5$, the total disc torque Γ exerted on a protoplanet held on a fixed circular orbit, which in the following we will refer to as the static torque, can be considered as the sum of the differential Lindblad torque, and the entropy-related corotation torque. In the limit where the corotation torque is fully unsaturated, Γ is given by (Paardekooper et al. 2010):

$$\gamma\Gamma/\Gamma_0 = -2.5 - 1.7\beta + 0.1\sigma + 7.9\frac{\xi}{\gamma}, \quad (6)$$

with $\Gamma_0 = (q/h_p)^2 \Sigma_p a^4 \Omega_p^2$. Here a is the planet semi-major axis and the subscript ‘‘p’’ indicates that quantities are evaluated at the orbital position of the planet. For $\xi = -1$, this gives $\gamma\Gamma/\Gamma_0 \sim -7.3$,

whereas $\gamma\Gamma/\Gamma_0 \sim 4.5$ for $\xi = 2$. For these two disc models, the total and entropy-related corotation torques have therefore the same sign, and the aim of this section is to examine whether in that case, a migrating protoplanet can reach migration rates that are significantly higher than those obtained by evaluating the static torque only. In isothermal discs a few times more massive than the MMSN, it has been shown that if the planet migrates in the direction set by the corotation torque, it can be subject to strong dynamical corotation torques and runaway effects can even be triggered under certain conditions (Paardekooper 2014).

The upper left panel of Fig. 1 shows, for the disc model with $\xi = -1$ and for various disc masses, the semi-major axis evolution of a $q = 10^{-5}$ planet initially located at $a_0 = 3$. In agreement with the above estimation of the total torque, the planet migrates inward in that case, and in the direction set by the static corotation torque since the entropy gradient is positive. Here, both the viscosity and thermal diffusivity are set to $\chi = 10^{-6}$, consistently with the assumption of a Prandtl number of unity. This value for the thermal diffusivity is chosen such that the entropy-related horseshoe drag is initially close to its unsaturated value. This is reached when the thermal diffusion timescale across the horseshoe region $\tau_d = x_s^2/\chi$ is approximately equal to half the libration timescale $\tau_{lib} = 8\pi a/(3\Omega_p x_s)$. However, it can be easily shown that $\tau_d/\tau_{lib} \propto a^{(1-3f)/2}$, which evaluates to $\tau_d/\tau_{lib} \propto a^{-0.55}$ for $f = 0.7$. Therefore, we expect the level of saturation of the corotation torque to increase as the planet migrates inward. In the lower left panel of Fig. 1 are compared, for the runs with $q_d = 0.005, 0.02$, the migration rates at different locations with those predicted from static

torques. Also plotted on this figure are the drift rates obtained assuming a fully unsaturated horseshoe drag, and which should therefore correspond, in principle, to the highest drift rates that could be reached by a migrating protoplanet. Clearly, the migration rates are significantly higher in the case where the planet is allowed to migrate, with values that appear to be even larger than the estimate given by assuming a fully unsaturated corotation torque.

The right panel of Fig. 1 presents the results of the simulations for the disc model with $\xi = 2$ and for which outward migration is expected. We note that the run with $q_d = 0.03$ serves for illustrative purpose only since $Q < 1$ for $R \geq 2$ in that case. Here $\tau_d/\tau_{lib} \propto a^{1.7}$, leading to an increase in the saturation of the corotation torque as the planet migrates outward. The main implication of this is that the total torque acting on the planet can eventually cancel at the location where the differential Lindblad torque and the saturated corotation torque have the same amplitude. An estimation for the location of this zero-torque radius a_S can be obtained by equating the diffusion and libration timescales across the horseshoe region. It is straightforward to show that this gives:

$$\frac{a_S}{a_0} \sim \left(40 \left(\frac{\chi}{a_0^2 \Omega_0} \right)^2 \left(\frac{h_0}{q} \right)^3 \right)^{\frac{1}{1.57}} \quad (7)$$

where Ω_0 is the angular velocity at the initial location of the planet. For $\chi = 10^{-6}$, $q = 10^{-5}$, and $f = -0.8$ we find $a_S/a_0 \sim 1.6$. Although not shown here, we find that such an estimation agrees fairly well with the value for the zero-torque radius deduced from runs with the planet held on a fixed orbit. The final evolution outcome for runs with $q_d \leq 0.01$ remains uncertain, but we can reasonably expect that the migration will ultimately be halted at $a \sim a_S$ for these cases. For $q_d \geq 0.02$, however, the migration rate continuously increases as the evolution proceeds, leading to the planet migrating outward very rapidly. This makes the planet pass through the location of the zero-torque radius predicted by static torques and rapidly reach the outer edge of the computational domain. In that case, the migration rate is again higher than what expected from the action of the Lindblad plus the fully unsaturated entropy-related corotation torque, as illustrated by the lower right panel of Fig. 1 which shows the drift rate as a function of radius for the simulation with $q_d = 0.02$. This result seems to indicate that in non-isothermal discs and provided the disc mass is high enough, a protoplanet can feel additional dynamical corotation torques as it migrates, similarly to what occurs in isothermal discs (Paardekooper 2014).

In Fig. 2 is presented the orbital evolution of a $q = 3.10^{-5}$ planet for the same disc model, except that both the viscosity and thermal diffusivity have been increased to $\nu = \chi = 10^{-5}$ to make sure that the underlying surface density profile is not altered by the presence of the planet. Eq. 7 predicts that outward migration should come to a halt at $a_S \sim 2.35$ in that case. Although it seems reasonable to claim that migration will stall close to this location in the simulation with $q_d = 0.005$, we see that the planet undergoes fast outward migration and crosses the location of the zero-torque radius in runs with $q_d \geq 0.01$. Here $q/h_0^3 \sim 0.8$, so that it is plausible that here, the occurrence of fast outward migration for lower disc masses might be related to the onset of non-linear effects, resulting in a boost of the corotation torque (Masset et al. 2006).

3.2 Coorbital mass deficit

In order to get some insight about the origin of the observed large drift rates, we display in Fig. 3 the perturbed surface density near

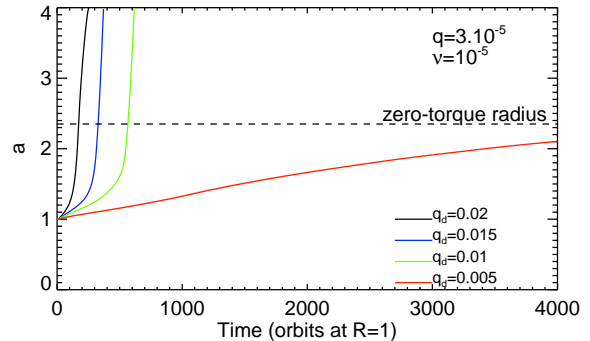


Figure 2. Time evolution of the semi-major axis of a planet with $q = 10^{-5}$ embedded in a non-isothermal disc with $\xi = 2$ and $\nu = \chi = 10^{-6}$, for various disc masses.

the planet at $t = 200$ orbits, for the disc model with $\xi = -1$ (left panel) and $\xi = 2$ (right panel). For $\xi = -1$ (resp. $\xi = 2$) the initial entropy gradient is positive (resp. negative) and dynamics in the horseshoe region yields a positive (resp. negative) surface density perturbation at the outward downstream separatrix whereas a negative (resp. positive) surface density perturbation is created at the inward downstream separatrix. Overplotted as black lines are a few streamlines which correspond to material that flows across the orbit by executing a single U-turn, whereas the overplotted white line shows the librating material bound to the planet. We see that the radial drift of the planet causes the horseshoe streamlines to be significantly distorted and to contract into a tadpole-like region. This arises because the planet drift rate \dot{a} is higher than the critical drift rate \dot{a}_f above which the planet migrates over a distance greater than the horseshoe width over one horseshoe libration time.

As the planet migrates, the material that flows across the orbit has always a positive feedback on migration, whereas librating material that moves with the planet has always a negative feedback on migration. However, in the case where the planet migrates in the direction set by the corotation torque, it is clear from Fig. 3 that the tadpole-like region tends to be underdense compared to the rest of the disc, resulting in a net positive feedback on migration, and possibly leading to high drift rates. We note that this effect cannot occur if the planet migrates in the opposite direction to that set by the corotation torque, since in that case the librating region would be over dense relative to the ambient disc, resulting in a significant negative feedback on migration.

Interestingly, the presence of such an underdense librating region at the leading side of the planet has also been observed in simulations of giant planets which undergo inward runaway migration (Artymowicz 2004; D'angelo & Lubow 2008). Here, it is worth noting that the low-density region does not result from the gap opening process but is rather due to radiative effects. Nevertheless, using the terminology employed in the framework of Type III migration, Fig. 3 shows that radiative effects can give rise to a coorbital mass deficit given by (Masset & Papaloizou 2003):

$$\delta m = 4\pi a x_s (\Sigma_s - \Sigma_h) \quad (8)$$

where Σ_s is the surface density at the upstream separatrix and Σ_h the mean surface density in the librating region. In order to provide an estimation for the coorbital mass deficit in the librating region, we make in the following the assumption that the only contribution to the density perturbation in the librating region results from entropy

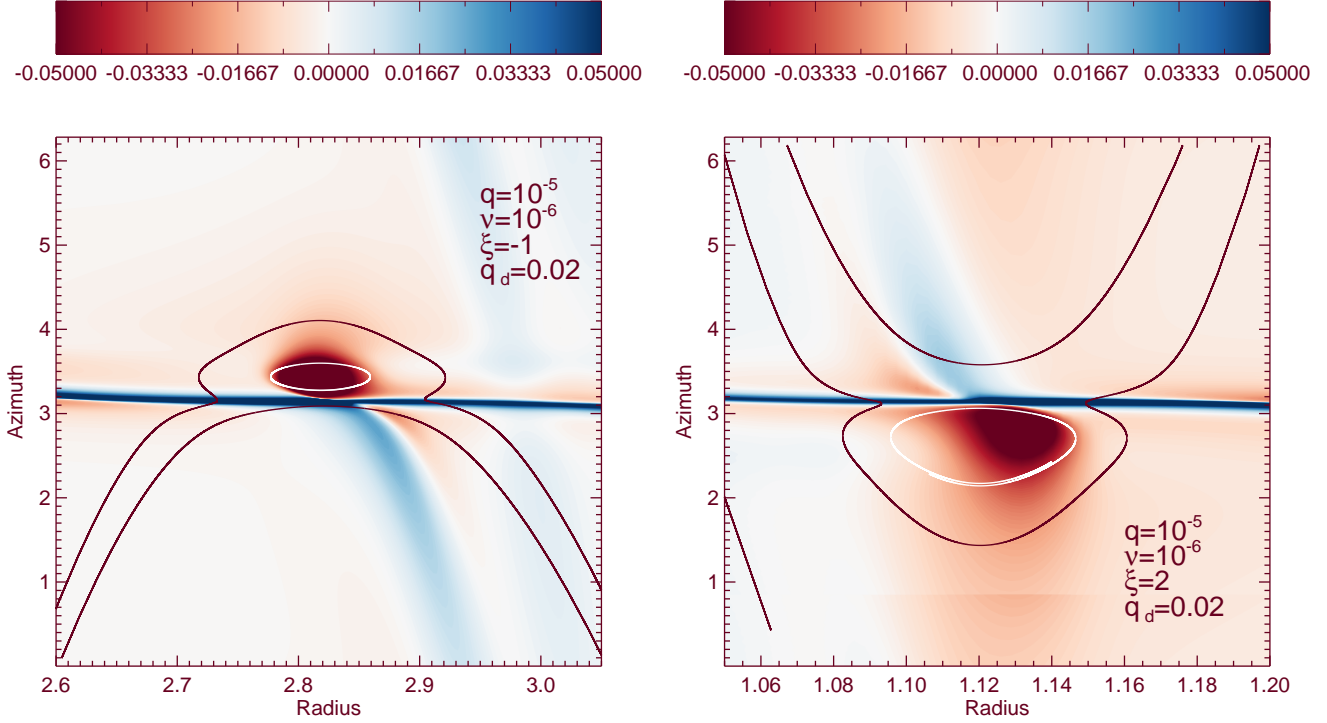


Figure 3. *Left panel:* Contours of the perturbed surface density at $t = 200$ orbits near the planet for the disc model with $\xi = -1$ and $q_d = 0.02$. Overplotted as white lines are a few streamlines that correspond to the librating trapped material that moves with the planet and which has therefore a negative feedback on migration. The black lines are streamlines that correspond to the material that flows across the orbit as the planet migrates and which has a positive feedback on migration. In the case where the planet migrates in the direction set by the corotation torque, the trapped region is gas depleted, yielding a net positive feedback on migration. *Right panel:* same but for the disc model with $\xi = 2$ and $q_d = 0.02$.

advection. In reality, however, the density perturbation features an additional contribution linked to the production of vortensity at the outgoing separatrix (Paardekooper et al. 2011). Ignoring this contribution gives the following expression for the surface density Σ_- in the librating region (Baruteau & Masset 2008; Paardekooper et al. 2011):

$$\Sigma_- = \Sigma_s \left(1 - 2 \frac{|\xi| x}{\gamma a} \right) \quad \text{for } 0 < x < x_s \quad (9)$$

Here, we have also ignored the radial density gradient and assumed that the corotation torque was initially unsaturated. This gives a mean surface density in the librating region:

$$\Sigma_h = \Sigma_s \left(1 - \frac{|\xi| x_s}{\gamma a} \right). \quad (10)$$

The coorbital mass deficit then becomes:

$$\delta m = 4\pi |\xi| x_s^2 \Sigma_s / \gamma \quad (11)$$

which shows that the coorbital mass deficit scales with the entropy gradient and the width of the horseshoe region. We note in passing that at the boundary corresponding to $\dot{a} \sim \dot{a}_f$, we expect the corotation torque exerted on the planet to be given by (e.g. Papaloizou et al. 2007):

$$\Gamma_{CR} = \frac{1}{2} \dot{a}_f \Omega_p a \delta m \quad (12)$$

Using the expression for the coorbital mass deficit given by Eq. 11,

the previous equation then becomes:

$$\Gamma_{CR} = \frac{3}{4} \frac{\xi}{\gamma} \Sigma_s x_s^4 \Omega_p^2 \quad (13)$$

so that we recover the standard expression for the entropy-related horseshoe drag (Baruteau & Masset 2008). For $\dot{a} > \dot{a}_f$, however, the expression for the unsaturated corotation torque given by Eq. 12 is no longer valid and should be modified (Papaloizou et al. 2007). In that case, we expect the corotation torque to be prevented from saturation since the horseshoe region does not longer extend to the full 2π in azimuth, so that phase-mixing cannot occur. In isothermal discs with a large-scale vortensity gradient, Ogilvie & Lubow (2006) found that drift rates with $\dot{a} > \dot{a}_f$ can even lead to torques that are much larger than the unsaturated value in absence of migration. They showed that this arises due to corotational torques caused by a vortensity asymmetry in the coorbital region between gas on the leading and trailing sides of the planet. In the limit of low viscosity, the trapped material tends to conserve its initial vortensity as the planet migrates, leading to a possibly significant vortensity contrast between the librating region and the local disc. In that case, the impact on migration depends in fact on the sign of the vortensity deficit (Paardekooper 2014) which is defined as:

$$\delta(\omega/\Sigma) = 1 - \frac{\omega_a/\Sigma_a}{\omega_0/\Sigma_0} \quad (14)$$

where ω_a/Σ_a is the local disc vortensity at the position of the planet and ω_0/Σ_0 the vortensity at the initial location of the planet. In the

case where the planet migrates in the direction set by the vortensity-related horseshoe drag, the vortensity deficit is positive and this yields a positive feedback on migration whereas if the planet migrates in the opposite direction to that set by the corotation torque, the vortensity deficit is negative and this gives rise to a negative feedback on migration (Paardekooper 2014).

Here, the appearance of the streamlines in Fig. 3, combined with the very high drift rates (higher than those expected from unsaturated torques) that have been reported in the previous section, strongly suggests that a mechanism similar to that presented in Ogilvie & Lubow (2006) is at work here. However, since there is no initial vortensity gradient inside the disc, we suggest the strong corotation torques acting on the planet as being generated by an entropy rather than a vortensity deficit between the trapped material and the ambient disc. For non-isothermal discs, we therefore make use of an entropy deficit δS that we define as:

$$\delta S = 1 - \frac{S_a}{S_0} \quad (15)$$

where S_a is the local disc entropy at the position of the planet and S_0 the disc entropy at its initial location. In the case where the entropy deficit is positive, the planet migrates in the direction set by the entropy-related horseshoe drag and an underdense region with an entropy excess compared to the local disc appears near the planet. As mentioned earlier, this yields a positive feedback on migration and possibly gives rise to high drift rates if the viscosity and thermal diffusivity are small enough so that the entropy excess in the librating region is conserved in the course of migration. In the case where the entropy deficit is negative, however, the librating region tends to be cooler and over dense relative to the ambient disc, resulting in a negative feedback on migration. In that case, we expect migration in non-isothermal discs to be strongly slowed down.

As mentioned earlier, we expect this mechanism to arise whenever the drift timescale across the horseshoe region is shorter than the libration time. This condition reads (Papaloizou et al. 2007):

$$\dot{a} > \dot{a}_f \quad (16)$$

with (Peplinski et al. 2008):

$$\dot{a}_f = \frac{3x_s^2 \Omega_p}{8\pi a} \quad (17)$$

Using Eq. 16, we can now estimate under which condition on the disc mass, horseshoe streamlines can be significantly distorted by the effect of the radial drift of the planet. The migration rate \dot{a} of the planet is (e.g. Paardekooper 2014):

$$\dot{a} = 2a \frac{\Gamma/\Gamma_0}{m_p \sqrt{GM_* a}} \Gamma_0 \quad (18)$$

Given that $\Gamma_0 = (q/h_p)^2 \Sigma_p a^4 \Omega_p^2$, the previous equation can be rewritten as:

$$\dot{a} = \frac{2}{\pi} (\Gamma/\Gamma_0) \frac{q q_d}{h_p^2} a \Omega_p \quad (19)$$

Substituting the latter expression in Eq. 16 and using $x_s \sim 1.2a \sqrt{q/h_p}$ we find that a protoplanet may enter a fast migration regime provided that:

$$\frac{q_d}{h_p} > \frac{0.27\gamma}{(\gamma\Gamma/\Gamma_0)}, \quad (20)$$

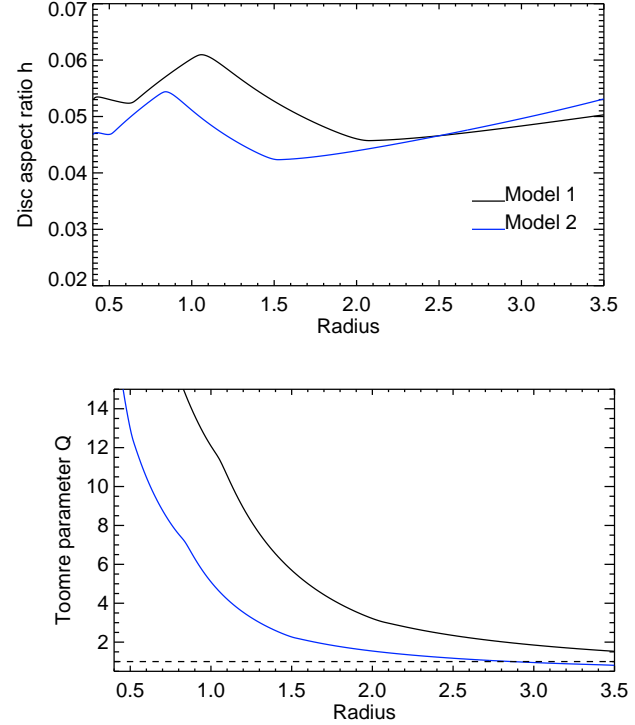


Figure 4. *Upper panel:* Disc aspect ratio as a function of radius for the two radiative disc models that are considered and with parameters given in Table 1. *Lower panel:* Toomre stability parameter as a function of radius for the two models. The dashed line corresponds to the gravitational stability limit.

or equivalently:

$$Q < \frac{3.7}{\gamma} (\gamma\Gamma/\Gamma_0), \quad (21)$$

where $Q = h/q_d$ is the Toomre parameter, and where $\gamma\Gamma/\Gamma_0$ is given by Eq. 6. For $\gamma = 1.4$ and using $\beta = \xi + (\gamma - 1)\sigma$, Eq. 6 reads:

$$\gamma\Gamma/\Gamma_0 = -2.5 + 3.9\xi - 0.6\sigma \quad (22)$$

Not surprisingly, this predicts that it is easier for the planet to enter the fast migration regime i) for high values of the entropy gradient, and ii) when the planet migrates inward and the entropy gradient is positive. This also shows that in the case where the planet migrates in the opposite direction to that predicted by the corotation torque, namely if ξ has a moderate and positive value, $\gamma\Gamma/\Gamma_0$ is of the order of unity and distortion of the horseshoe streamlines occurs only provided that the disc is relatively massive. For the disc model with $\xi = -1$, we note that Eq. 20 predicts fast migration for $q_d \geq 0.003$ which is in perfect agreement with the results of the simulations. In the case with $\xi = 2$, however, Eq. 20 predicts fast migration for $q_d \geq 0.005$ whereas the right panel of Fig. 1 shows fast migration for $q_d > 0.01$. This discrepancy possibly arises because the expression given by Eq. 20 does not take into account possible saturation effects. We therefore expect this estimation to slightly underestimate the critical disc mass above which fast migration should occur.

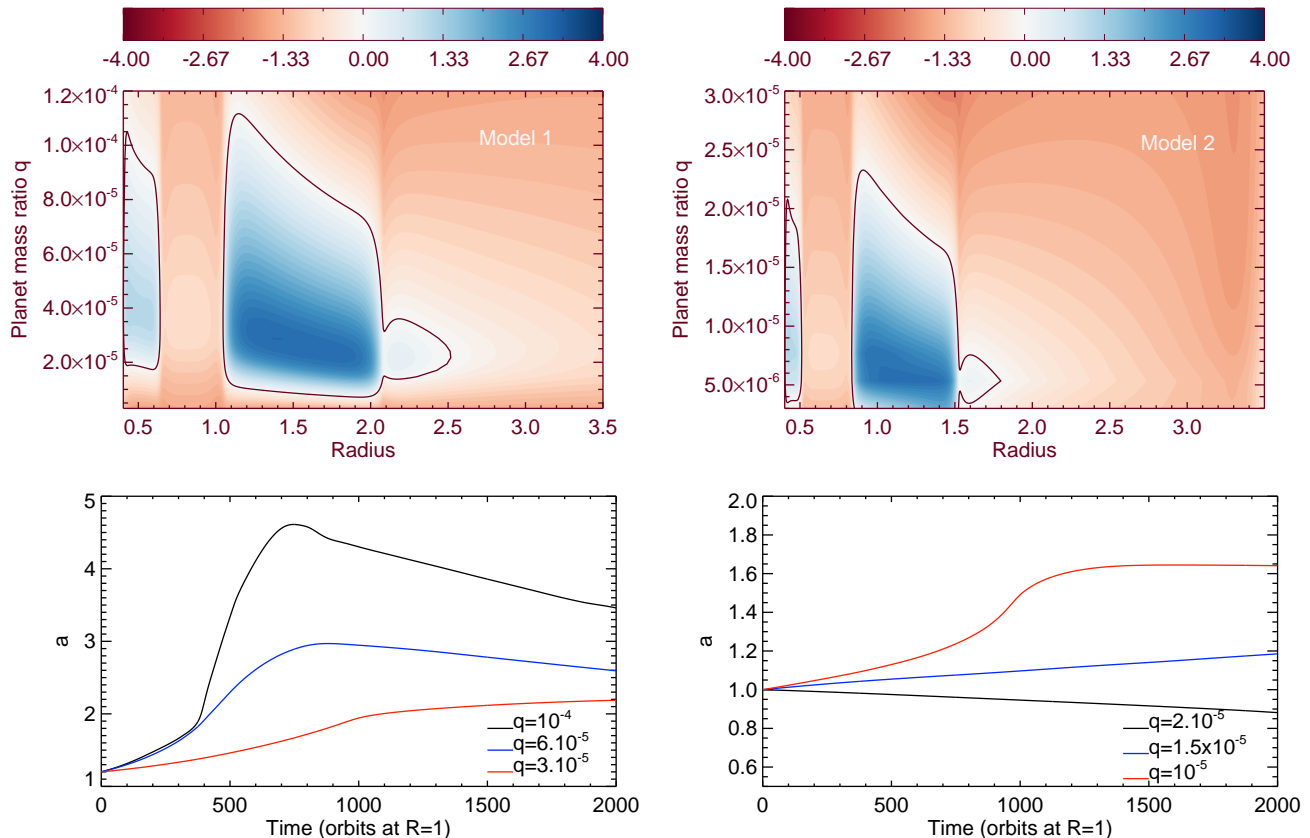


Figure 5. *Upper panel:* Contour plots showing, for the two radiative disc models, the disc torque as a function of planet mass and planet radial location. This has been derived using the analytical formulae of Paardekooper et al. (2011). *Lower panel:* this shows, for the two radiative discs, the time evolution of the semi-major axes of planets of different masses and that are initially located in the region where outward migration is expected to proceed.

4 RADIATIVE DISC MODELS

4.1 Results

We now turn to the case of equilibrium radiative discs for which the thermodynamical state is determined by the balance between viscous heating, stellar irradiation, and radiative cooling. We plot in Fig. 4 the disc aspect ratio (upper panel) and Toomre stability parameter (lower panel) as a function of radius for the two models we consider. We remind the reader that the disc parameters for the two models can be found in Table 1. For Model 1, the structure in the disc aspect ratio is very similar to that of stellar equilibrium discs (SED) obtained using 3D hydrodynamical simulations (see for example Fig. 1 in Lega et al. 2015). In the inner disc, viscous heating dominates over stellar irradiation and opacity transitions create bumps in H/R at $R \sim 0.6$ and $R \sim 1$ (Bitsch et al. 2013, 2014). In the outer parts of the disc, however, stellar irradiation is the main source of heating, leading to a flared disc with $H/R \propto R^{2/7}$ for $R \gtrsim 2$. For Model 2, the aspect ratio is slightly smaller due to the lower value for the viscosity but the radial profile of H/R looks similar to that for Model 1. For both models, the torque as a function of planet mass and orbital distance is presented in the upper panel of Fig. 5. Following Bitsch et al. (2013), these migration maps have been obtained using the analytical formulae of Paardekooper et al. (2011) which include saturation effects for the corotation torque. Here, the black lines delimitate the regions in the disc where outward migration should occur. As expected, Type I migration is directed inward in the flared parts of the disc

where the entropy gradient is positive, yielding a negative entropy-related corotation torque. In the regions where the disc aspect ratio decreases with radius, however, the entropy gradient tends to be negative, and this can possibly lead to outward migration if the corotation torque is not saturated and the entropy gradient steep enough. Because the thermal diffusion timescale tends to increase with radius, outward migration will proceed in that case until the planet reaches the zero-torque radius where the saturated corotation torque counterbalances the Lindblad torque. As mentioned in Sect. 3.1, this occurs when the thermal diffusion timescale is approximately equal to the libration timescale in the horseshoe region. Moreover, since the libration period decreases as the planet mass increases, the zero-torque radius set by saturation tends to be located closer in for heavier planets, which is clearly seen in the upper panel of Fig. 5. For Model 1 (resp. Model 2), protoplanets with $q \lesssim 6 \times 10^{-5}$ (resp. $q \lesssim 1.6 \times 10^{-5}$) would have their zero-torque radius located in the flared part of the disc where the entropy gradient is positive. For this mass range, the location of the zero-torque radius becomes almost mass-independent (Cossou et al. 2013) and rather corresponds to the transition between the viscous heating dominated regime and the stellar heating dominated region. This is located at $R \sim 2$ for Model 1 while it is located at $R \sim 1.5$ for Model 2.

We note that these migration maps have been computed from analytical formulae that are valid for planets held on a fixed circular orbit only. Returning to Fig. 4, however, we see that the Toomre stability parameter can reach values in the range

$2.5 < Q < 5$ in the regions where outward migration is expected to occur. From the discussion presented in Sect. 3.2, it cannot be excluded that the criterion given by Eq. 21 is fulfilled in this case, and that drift rates significantly higher than those predicted by static torques can be reached. More precisely, for both models, the entropy gradient in the region of outward migration is estimated to be such that $\xi \sim 1.8$, which gives $\gamma\Gamma/\Gamma_0 \sim 4$ from Eq. 22. The condition given by Eq. 21 therefore becomes $Q \lesssim 10$, which is clearly fulfilled for Model 2, and for Model 1 as well in regions with $R \gtrsim 1.3$ (see lower panel of Fig. 4).

For Model 1, we present in the lower left panel of Fig. 5 the semi-major axis as a function of time for planets with $q = 3 \times 10^{-5}, 6 \times 10^{-5}, 10^{-4}$ and initially located at $a_0 = 1.1$, namely at a location where outward migration is expected to occur for this mass range. The orbital evolution of the $q = 3 \times 10^{-5}$ protoplanet is in close agreement with that predicted from the upper panel of Fig. 5, involving outward migration until the zero-torque radius located at $R \sim 2.1$ is reached. For $q = 6 \times 10^{-5}, 10^{-4}$, however, the evolution differs significantly to what expected from the migration map. The drift rates for these cases appear to be significantly higher than those estimated using static saturated or unsaturated corotation torques, leading the planets to migrate outward well beyond the zero-torque radius. This is exemplified in Fig. 6 where we plot the planet drift rate as a function of radius for both cases. For the run with $q = 10^{-4}$, it is clear that the planet enters a very fast migration regime once $R \sim 1.8$, which corresponds to a value for the Toomre parameter of $Q \sim 4$ (see the lower panel of Fig. 4). We suspect this value to correspond to the limit below which the mechanism presented in Sect. 3.2 is at work. To demonstrate that this is indeed the case, we show in Fig. 7 a series of surface density plots at different times for this simulation. At early times, there is a negative (resp. positive) surface density perturbation at the outward (resp. inward) downstream separatrix due to the negative entropy gradient, and the horseshoe region is clearly visible. At $t \sim 350$ orbits, namely just before the planet starts its fast outward migration, an underdense librating region has appeared, suggesting thereby that the condition given by Eq. 16 is verified at that time. As mentioned in Sect. 3.2, this can yield a strong positive corotation torque which is responsible for the high drift rates observed. As can be seen in the third panel of Fig. 7, the trapped region progressively shrinks in the course of migration and a part of the coorbital mass deficit can be lost, resulting in the planet migrating inward again at later times. Interestingly, we note that a similar process prevents outward runaway migration (Masset & Papaloizou 2003) to be sustained over long timescales. Here, thermal diffusion acts also against fast migration since it makes the trapped region cool down, leading to a slight increase in the surface density. Once the planet migrates inward again and evolves in the flared part of the disc, the thermodynamical state of the disc is close to the isothermal limit so that radiative effects can not lead to the formation of an underdense librating region near the planet, resulting in the planet migrating under the action of static torques only.

For Model 2, the orbital evolution of planets with $q = 10^{-5}, 1.5 \times 10^{-5}, 2 \times 10^{-5}$ is shown in the lower right panel of Fig. 5. Outward migration here occurs for $q \leq 1.5 \times 10^{-5}$ whereas saturation of the corotation torque makes the $q = 2 \times 10^{-5}$ protoplanet migrate inward. In the latter case, we note that this does not agree with the migration map in the upper panel of Fig. 5 which predicts outward migration for $R \lesssim 1.2$. Inspection of this migration

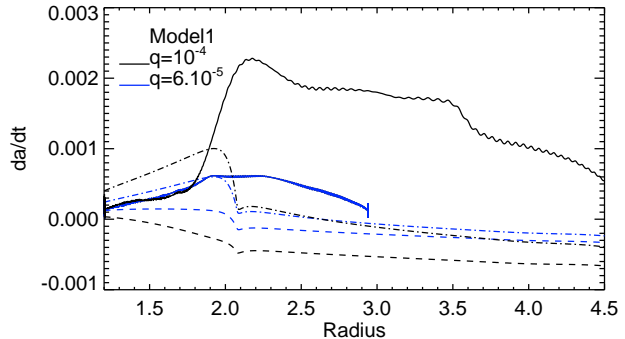


Figure 6. Drift rate as a function of the radial location of the planet for the simulations with $q = 6 \times 10^{-5}, 10^{-4}$ and for the radiative disc corresponding to Model 1. The dashed line represents the drift rate that is obtained using the formulae of Paardekooper et al. (2011) for the disc torque, whereas the dot-dashed line represents the drift rate predicted assuming a fully unsaturated corotation torque.

map also reveals that compared to the case with $q = 1.5 \times 10^{-5}$, the level of saturation is clearly initially smaller for a planet mass with $q = 10^{-5}$. The resulting faster outward migration makes the $q = 10^{-5}$ body rapidly reach regions with relatively low Q values. Analysis of the streamlines reveals that the horseshoe region is destroyed at $t \sim 700$ orbits, at which time the planet has migrated to a disc region where $Q \sim 3.5$. Again, this is fairly consistent with the estimation given by Eq. 21. From that time, the planet undergoes an episode of fast migration due to the effect presented above, but becomes ultimately trapped at the zero-torque radius located at the transition between the viscous heating dominated and stellar heating dominated regimes. In agreement with the discussion of Sect. 3.2, we find that the typical drift rates during fast migration can be higher than those predicted assuming a fully unsaturated corotation torque, as illustrated by Fig. 8 which shows for this run the drift rate of the planet as a function of its radial location in the disc.

For $q = 6 \times 10^{-5}$, we mention that continuation of the run indicates that the planet does not appear to experience fast migration, in spite of the fact that it can evolve in disc regions with $Q \sim 3.5$. This possibly arises because, as mentioned above, the corotation torque is quite saturated in that case, resulting in a low contrast of entropy initially between the trapped material and the local disc.

4.2 Implication for the formation of giant planet cores

It has been suggested that the zero-torque radius may represent an ideal site for the growth of giant planet cores through giant impacts between Earth-mass embryos (Lyra et al. 2010; Hasegawa & Pudritz 2011). Pierens et al. (2013) have studied the evolution of multiple planets of a few Earth masses which migrate convergently toward a convergence zone located at the transition between two different opacity regimes. They found that the embryos tend to form a stable resonant chain that protect them from close encounters with other bodies, preventing thereby the subsequent formation of giant planet cores. In the case of a large number of initial embryos or if the effects of disc turbulence are included these resonant configurations can be disrupted, but the formation of massive cores remains marginal. In a subsequent study, Zhang et al. (2014) focused on the case where the zero-torque radius is located at the transition between the inner viscously heated part of the disc and the outer irradiated region. They found that in massive discs with accretion

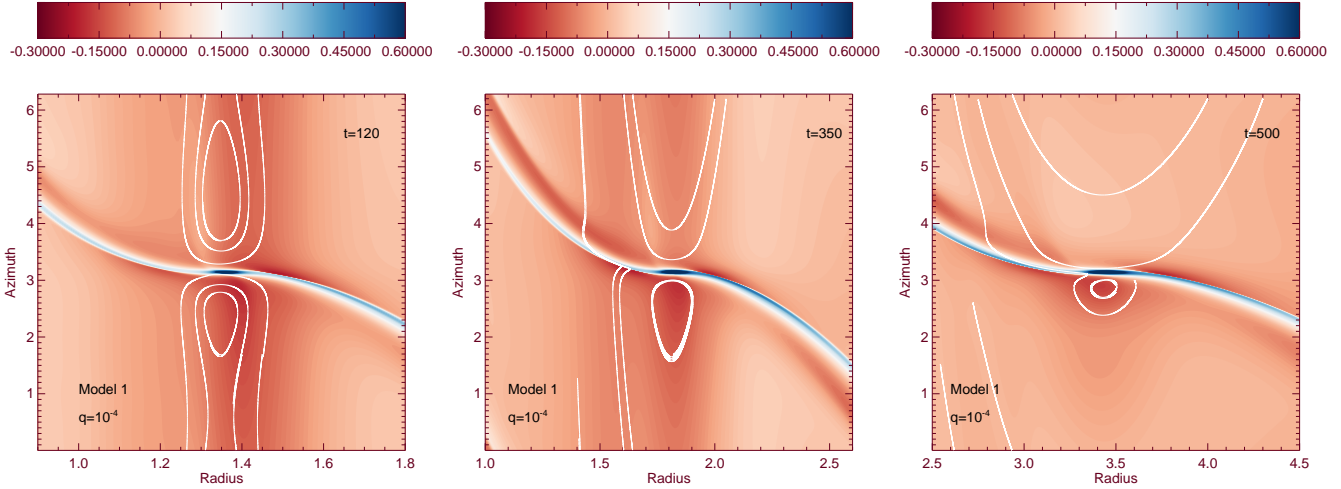


Figure 7. Maps of the perturbed surface density at $t = 120, 350, 500$ orbits for the simulation with $q = 10^{-4}$ and for the radiative disc corresponding to Model 1.

rates $\dot{M} \sim 10^{-7} M_{\odot}/\text{yr}$ the resonant barriers that are formed can be broken, enabling the formation of massive cores.

In massive discs, the mechanism presented in Sect. 3.2 may also facilitate the disruption of resonances at convergence zones and consequently promote collisions between embryos. To investigate this issue in more details, we have examined the evolution of four planets with $q = 10^{-5}$ embedded in the disc corresponding to Model 2, and located in the vicinity of the zero-torque radius at $R \sim 1.5$. According to the results presented in the previous section, the bodies located inside the zero-torque radius are expected to rapidly migrate outward.

Here, we used a setup similar to that presented in Pierens et al. (2013), with two embryos initially located on each side of the zero-torque radius and separated by $4.5 R_{mH}$, where R_{mH} is the mutual Hill radius. The protoplanets are initially set on moderately inclined orbits, and a prescription for the rate of inclination damping due to the interaction with the disc is employed (see Pierens et al. 2013).

Fig. 9 shows the time evolution of the semi major axis for the 4 protoplanets. At early times, the two innermost (resp. outermost) bodies located inside the zero-torque radius undergo outward (resp. inward) migration, as expected. For the two innermost bodies, fast outward migration is observed, in agreement with the results of the previous section. This causes the embryo initially located at $a_0 = 1.1$ (blue) to rapidly reach the zero-torque radius and to enter in a 9 : 8 resonance with the third planet (black) at $t \sim 700$ orbits. The inward migrating fourth planet (red) then catches up with these two bodies and enter in a 9 : 8 resonance with them. This resonant chain is however subsequently destabilized due to the fast outward migration of the first body (green), resulting in a physical collision between the two outermost planets at $t \sim 1000$ orbits. The $6.6 M_{\oplus}$ planet that is formed at that time by this process subsequently migrates inward until it reaches the zero-torque radius at $R \sim 1.5$. Regarding the two innermost embryos, they undergo a series of orbital exchanges inside the zero-torque until they collide at $t \sim 2800$ orbits, leading again to the formation of a $6.6 M_{\oplus}$ planet. From the migration map corresponding to model 2, we expect this body to slowly migrate inward at later times until it reaches the zero-torque radius set by saturation and which is located at $R \sim 1.2$ for such a planet mass.

This result seems to indicate that in relatively massive discs for

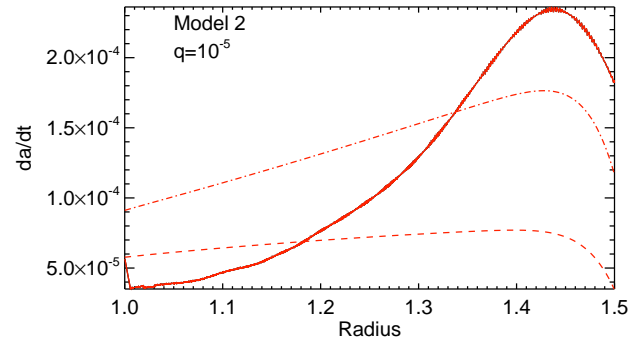


Figure 8. Drift rate as a function of the radial location of the planet for the simulations with $q = 10^{-5}$ and for the radiative disc corresponding to Model 2. The dashed line represents the drift rate that is obtained using the formulae of Paardekooper et al. (2011) for the disc torque, whereas the dot-dashed line represents the drift rate predicted assuming a fully unsaturated corotation torque.

which the condition given by Eq. 21 is fulfilled, fast convergent migration of low-mass embryos may indeed enhance the formation of massive cores through collisional growth of low-mass bodies. We will address in a future publication the issue of the dependence of these results on the disc model and initial mass of the embryos, and investigate whether or not giant planet cores may indeed be formed by this process.

5 DISCUSSION AND CONCLUSION

In this paper, we have presented the results of hydrodynamic simulations of the orbital evolution of embedded low-mass planets in non-isothermal and radiative discs. A main aim of this study is to examine the dependence of the planet drift rate on the disc mass and entropy gradient inside the disc, with particular emphasis put on the possible role of dynamical corotation torques. We consider non-barotropic discs with an initial radial entropy gradient, and in which both the thermal diffusion coefficient and viscosity are con-

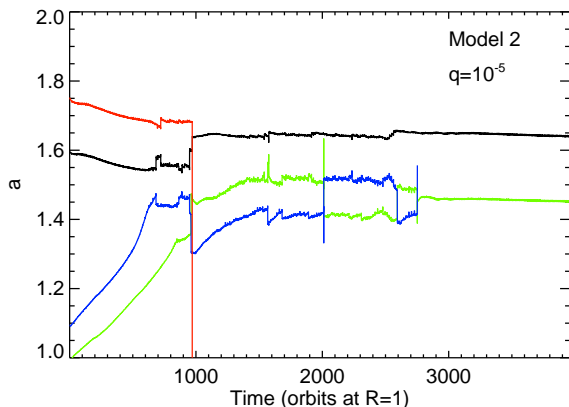


Figure 9. Orbital evolution of four embryos with mass ratio $q = 10^{-5}$ initially located near the transition between the viscous heating dominated and stellar heating dominated regimes, for the radiative disc model corresponding to model 2.

stant. We also investigate the case of radiative disc models that include the effect of viscous heating, stellar irradiation and radiative cooling. For non-isothermal disc models with an initial non-zero entropy gradient and zero vortensity gradient, we find that the drift rates of a migrating protoplanet can be, under certain conditions, much higher than those expected from classical formulae for the disc torque. We observe that these can even be higher than those expected assuming a fully unsaturated horseshoe drag. This arises provided that i) the Toomre stability parameter is less than a critical value that depends on the entropy gradient inside the disc and which is given by Eq. 21 and ii) the planet migrates in the direction set by the entropy-related horseshoe drag. If condition i) is satisfied, the horseshoe region of the planet does not extend to the full 2π in azimuth and rather contracts into a tadpole-like region (Papaloizou et al. 2007). This region is bound to the planet and has therefore a negative feedback on migration. It is located at the leading side of the planet if the latter migrates inward, whereas it is located at trailing side of the planet if migration is inward. However, if condition ii) is also verified, the trapped material shows an entropy excess and becomes underdense relative to the ambient disc as the disc tries to maintain a pressure balance. In that case, the main contribution to the corotation torque comes from the material that flows across the orbit as the planet migrates and which yields a positive feedback on migration. This can make the planet enter in a fast migration regime, provided that the viscosity and thermal diffusivity are small enough so that the entropy excess in the trapped region tends to be conserved in the course of migration.

As a side result, we find that an outward migrating planet that enters such a fast migration mode can pass through the location of the zero-torque radius due to saturation effects, in agreement with the results of Paardekooper (2014) in isothermal discs.

Our simulations for radiative disc models essentially confirm these findings. For a stellar equilibrium disc with constant viscosity $\nu = 10^{-5}$ and disc mass equivalent to 5 times the Minimum Mass Solar Nebula (MMSN) at 5 AU, planets with mass ratio in the range $6 \times 10^{-5} < q < 10^{-4}$ are observed to enter a fast migration regime in the region $5 < R < 10$ AU where outward migration should proceed according to the corresponding migration map (see Fig. 5). In agreement with the analytical estimation given by Eq. 21, this occurs once the Toomre stability parameter becomes smaller than the

critical value $Q \sim 3 - 4$. From that time, strong corotation torques make the planet not only pass through the location of the zero-torque radius set by saturation, but also migrate well beyond the boundary corresponding to the transition between the viscous heating dominated regime and the stellar heating dominated regime. For example, we observe that fast outward migration of Neptune-mass planets can proceed until the planet reaches $R \sim 20$ AU, whereas migration contours predict inward migration outside 7 AU. For a model with $\nu = 10^{-6}$ and disc mass equivalent to 2.5 times the MMSN at 5 AU, we find that the mechanism presented above can strongly affect the outward migration of protoplanets with $q \sim 10^{-5}$ (equivalent to $3.3 M_{\oplus}$). In that case, it appears that the drift rate is again higher than the one expected assuming a fully unsaturated corotation torque, but the planet becomes ultimately trapped at the transition between the viscous heating dominated and stellar heating dominated regimes. For $q = 10^{-5}$, we have examined the impact of this fast migration regime on the orbital evolution of multiple planets that convergently migrate at this transition. We find that the high drift rates that are achieved in the course of outward migration may help in disrupting the resonant chains that are established between embryos. The consequence is that the process of giant core growth by collisions of low-mass bodies may be easier if these embryos undergo fast migration, but this needs to be investigated in more details.

A major simplification of this work resides in the fact that we have not considered the effect disc self-gravity. However, we have seen that the typical value for the Toomre stability parameter below which fast migration is triggered is typically $Q \sim 3 - 4$ in radiative discs. For such a value, the shift in the positions of the Lindblad resonances caused by self-gravity (Pierens & Huré 2005) is expected to lead to a Lindblad torque which is $\sim 15\%$ stronger in comparison with the case where self-gravity is discarded (Baruteau & Masset 2008). In the case where the planet migrates outward (resp. inward), we therefore expect Eq. 21 to slightly underestimate (resp. overestimate) the value for Q below which the horseshoe streamlines become significantly distorted by the radial drift of the planet. Clearly, additional self-gravitating simulations are required to definitely assess how these results are impacted by including the effect of the disc self-gravity. This issue will be examined in a future publication.

ACKNOWLEDGMENTS

We thank A. Morbidelli, R. Nelson and S. Raymond for useful discussions. Computer time for this study was provided by the computing facilities MCIA (Mésocentre de Calcul Intensif Aquitain) of the Université de Bordeaux and by HPC resources of Cines under the allocation c2015046957 made by GENCI (Grand Equipement National de Calcul Intensif). We thank the Agence Nationale pour la Recherche under grant ANR-13-BS05-0003 (MOJO).

REFERENCES

- Artymowicz, P. 2004, Debris Disks and the Formation of Planets, 324, 39
- Baruteau, C., & Masset, F. 2008, ApJ, 672, 1054
- Baruteau, C., & Masset, F. 2013, Lecture Notes in Physics, Berlin Springer Verlag, 861, 201
- Bell, K. R., & Lin, D. N. C. 1994, ApJ, 427, 987

- Bitsch, B., Crida, A., Morbidelli, A., Kley, W., & Dobbs-Dixon, I. 2013, *A&A*, 549, A124
- Bitsch, B., Morbidelli, A., Lega, E., & Crida, A. 2014, *A&A*, 564, A135
- Coleman, G. A. L., & Nelson, R. P. 2014, *MNRAS*, 445, 479
- Cossou, C., Raymond, S. N., & Pierens, A. 2013, *A&A*, 553, L2
- Cossou, C., Raymond, S. N., Hersant, F., & Pierens, A. 2014, *A&A*, 569, A56
- Cumming, A., Butler, R. P., Marcy, G. W., et al. 2008, *PASP*, 120, 531
- D'Angelo, G., & Lubow, S. H. 2008, *ApJ*, 685, 560
- de Val-Borro, M., Edgar, R. G., Artymowicz, P., et al. 2006, *MNRAS*, 370, 529
- Goldreich, P., & Tremaine, S. 1979, *ApJ*, 233, 857
- Günther, R., Schäfer, C., & Kley, W. 2004, *A&A*, 423, 559
- Hasegawa, Y., & Pudritz, R. E. 2011, *MNRAS*, 417, 1236
- Hayashi, C. 1981, *Progress of Theoretical Physics Supplement*, 70, 35
- Hellary, P., & Nelson, R. P. 2012, *MNRAS*, 419, 2737
- Kley, W. 1989, *A&A*, 208, 98
- Kley, W., & Crida, A. 2008, *A&A*, 487, L9
- Lega, E., Morbidelli, A., Bitsch, B., Crida, A., & Szulagyi, J. 2015, [arXiv:1506.07348](https://arxiv.org/abs/1506.07348)
- Lissauer, J. J., Ragozzine, D., Fabrycky, D. C., et al. 2011, *ApJS*, 197, 8
- Lovis, C., Ségransan, D., Mayor, M., et al. 2011, *A&A*, 528, A112
- Lyra, W., Paardekooper, S.-J., & Mac Low, M.-M. 2010, *ApJL*, 715, L68
- Masset, F. 2000, *A&AS*, 141, 165
- Masset, F. S. 2002, *A&A*, 387, 605
- Masset, F. S., & Papaloizou, J. C. B. 2003, *ApJ*, 588, 494
- Masset, F. S., Morbidelli, A., Crida, A., & Ferreira, J. 2006, *ApJ*, 642, 478
- Masset, F. S., D'Angelo, G., & Kley, W. 2006, *ApJ*, 652, 730
- Masset, F. S., & Casoli, J. 2009, *ApJ*, 703, 857
- Masset, F. S., & Casoli, J. 2010, *ApJ*, 723, 1393
- Menou, K., & Goodman, J. 2004, *ApJ*, 606, 520
- Mordasini, C., Alibert, Y., & Benz, W. 2009, *A&A*, 501, 1139
- Mordasini, C., Alibert, Y., Georgy, C., et al. 2012, *A&A*, 547, A112
- Ogilvie, G. I., & Lubow, S. H. 2006, *MNRAS*, 370, 784
- Paardekooper, S.-J., & Papaloizou, J. C. B. 2008, *A&A*, 485, 877
- Paardekooper, S.-J., & Papaloizou, J. C. B. 2009, *MNRAS*, 394, 2283
- Paardekooper, S.-J., Baruteau, C., Crida, A., & Kley, W. 2010, *MNRAS*, 401, 1950
- Paardekooper, S.-J., Baruteau, C., & Kley, W. 2011, *MNRAS*, 410, 293
- Paardekooper, S.-J. 2014, *MNRAS*, 444, 2031
- Papaloizou, J. C. B., Nelson, R. P., Kley, W., Masset, F. S., & Artymowicz, P. 2007, *Protostars and Planets V*, 655
- Pepliński, A., Artymowicz, P., & Mellema, G. 2008, *MNRAS*, 386, 179
- Pierens, A., & Huré, J.-M. 2005, *A&A*, 433, L37
- Pierens, A., Baruteau, C., & Hersant, F. 2012, *MNRAS*, 427, 1562
- Pierens, A., Cossou, C., & Raymond, S. N. 2013, *A&A*, 558, A105
- Tanaka, H., Takeuchi, T., & Ward, W. R. 2002, *ApJ*, 565, 1257
- van Leer, B. 1977, *Journal of Computational Physics*, 23, 276
- Zhang, X., Liu, B., Lin, D. N. C., & Li, H. 2014, *ApJ*, 797, 20